ASCENT PROBLEMS OF SOUNDING ROCKETS

By N. L. Crabill

Langley Research Center
Langley Field, Va., U.S.A.

For Presentation at AGARD Specialists Meeting
on Use of Rocket Vehicles in Flight Research

Scheveningen, The Netherlands
July 18-21, 1961

NATIONAL AERONAUTICS AND
SPACE ADMINISTRATION
WASHINGTON

ASCENT PROBLEMS OF SOUNDING ROCKETS

By N. L. Crabill*

Sounding rockets are rocket vehicles designed to carry scientific payloads above the sensible level of the atmosphere. The trajectories of these rockets are very steep, and as a consequence, two important problems arise. These problems are:

(1) The dynamic stability of the entire vehicle system as it leaves the atmosphere

(2) The effect of winds on the initial part of the trajectory of such an unguided vehicle.

This paper will describe briefly the results of an NASA attempt to cope with these two problems on a particular rocket vehicle.

The Dynamic Stability Problem

The dynamic stability problem of sounding rockets arises from the rapid decrease in air density with time, and even occurs in flights of vehicles which exhibit positive short-period damping. In a sense it is a problem involving the damping of a phugoid mode, and is the inverse of the well-known dynamic stability problem associated with reentry, reference 1. Zimmerman, reference 2, indicated that under suitable conditions a nonrolling vehicle would leave the atmosphere with a tumbling motion. With small spin, the spin frequency inevitably coincides with the short-period frequency if the vehicle goes high enough, resulting in large changes in vehicle attitude. If the event occurs at high dynamic pressures, large transverse loads may result; if it occurs near separation in a multistage rocket flight, large dispersions arise. The problem is not new; it was noticed by the Germans in 1938, reference 3, and studied in some detail by Phillips in 1948, reference 4, and later by Nicolaides, reference 5, Nelson, reference 6, and Enkenhus and Bilodeau, reference 7. Most of these studies are concerned with steady-state conditions. Very little has been reported on the transients encountered in traversing the resonance region as a sounding rocket does. This problem was investigated in the present study by analyzing the actual motions and loads of the SHOT PUT vehicle first stage with various roll fin deflections by means of a six-degree-of-freedom simulation.

The six equations of rigid body motion utilized in the investigation are fully explained in reference 8 and are presented in the written version of this paper. Some of the important assumptions involved are shown in figure 1. All of the inertial terms are used. However, in the forcing functions the assumption of equal aerodynamic stability in pitch and yaw

---

*Aerospace Technologist.

is made, and no allowance is made for the induced rolling-moment effect. In programming these equations for use on the digital computer, the aerodynamic forces and moments were allowed to vary with resultant angle of attack and Mach number. Aerodynamic asymmetries in pitch and yaw were permitted.

The SHOT PUT vehicle configuration, trajectory, and short-period characteristics are shown in the next few figures. Figure 2 shows that it is a two-stage solid-propellant rocket weighing about 11,000 pounds at lift off. The first-stage burns for about 32 seconds; the second contained within the fairing, burns for about 42 seconds. The large 15 ft^2 fins have a flat sided wedge airfoil of 8^o total angle. Two auxiliary rockets are used to provide additional acceleration for the first 2 seconds to overcome the problems resulting from low initial acceleration and a zero length launcher. This is not a particularly efficient rocket, but it proved to be a useful assembly of components designed for other purposes.

Figure 3 shows the nominal trajectory in space. The launch angle is 78^o, and first-stage burnout occurs at 32.5 seconds and 71,000-foot altitude. A long coast period of the entire combination is necessary to get the unstable second stage out of the atmosphere before separation which occurs at 80 seconds and 200,000 feet. The dynamic stability problems of current interest occur in this ascent phase of flight, before the second-stage separation. Second-stage apogee is about 1,200,000 feet and impact occurs at about 550 nautical miles.

The first-stage time histories of acceleration, velocity, and dynamic pressure are given in figure 4. Notice the 12g initial acceleration imparted largely by the auxiliary rockets. Without these rockets the initial acceleration would be about 4.5g and the vehicle would be too sensitive to winds. The maximum first-stage velocity of about 4,000 ft/sec occurs at 28 seconds, and the maximum dynamic pressure is about 4,500 lb/ft^2 at 23 seconds. The decreasing dynamic pressure from 23 seconds onward proved to be a serious source of dynamic stability trouble.

Figure 5 shows the calculated first-stage short-period oscillation characteristics plotted against time. The average damping ratio during powered flight is about 0.085. The frequency reaches a maximum of 13.5 radians/sec at 12 seconds and decreases asymptotically to zero thereafter. The general timewise variation of these parameters is typical of many sounding rockets.

Figure 6 portrays the asymmetries assumed in order to generate the motions and loads during the simulation of the ascent phase of the SHOT PUT vehicle. The arrows indicate the direction of rotation of the vehicle nose due to the action of the indicated misalignment. The

angular orientations of the fin and fairing misalignments were chosen to represent a reasonable "worst case," but not the "worst possible" case. The magnitudes of these misalignments are values that experience indicates we can maintain most of the time, if careful checks of the vehicle components and assemblies are made. The roll deflections deserve special comment. The fins were straight-sided wedges manufactured with special care to be flat within $\pm 1/10^{\circ}$ at any point. It was estimated that under these conditions, the resultant probable error in setting four fins in roll would be no better than $\pm 1/16^{\circ}$.

The ratio of instantaneous roll rate p to the instantaneous short-period frequency ω, is shown in this figure for the three cases. With a fin roll deflection of $1/16^{\circ}$, resonance is indicated at 50 seconds. The corresponding times with deflections of 1° and 2° are 18 and 12 seconds, respectively. Note that the 2° case remains near resonance from the start to about 16 seconds. At 80 to 100 seconds, near the time for second-stage separation, the ratios for all three cases are far removed from resonance.

The space motions for two cases are shown in figure 8. Motion in space is indicated by plotting θ versus ψ with time as a parameter, where θ is the X-axis elevation angle in the plane of X and the earth, ψ is the X-axis azimuth angle measured from the down range axis in the plane of the earth. With a deflection of $1/16^{\circ}$, note that very large angular displacements and rates develop toward the end of the coast period. This motion is completely unsatisfactory for a two-stage vehicle because of the resulting large dispersions of the second stage. With a deflection of 2°, a very satisfactory motion is indicated near the end of the coast phase, but large amplitudes and possibly loads are experienced from $t = 7$ to 15 seconds. The pronounced left yaw exhibited with a deflection of 2° can be explained readily as the gyroscopic precession resulting from the spin and the small stable aerodynamic pitching moment developed in the θ plane due to the curvature of the trajectory and the near constant attitude of the vehicle due to spin.

Figure 9 shows the resultant transverse load factor at the center of gravity for the three cases and indicates that with a fin roll deflection of $1/16^{\circ}$, a maximum of 3.0g occurs at about 25.0 seconds. The no spin trajectory (not shown) gives the same load factor up to $t \approx 30$ seconds. The corresponding maxima with 1° and 2° are 4.1g at 20 seconds and 1.4g at 13 seconds, respectively. For 1° and 2°, the maxima occur slightly after the corresponding times for $p/\omega = 1$, in figure 7. These transient results show trends consistent with the steady-state results of Enkenhus and Bilodeau, reference 7, who show that for steady resonance, the amplification factor for "rolling trim" compared to "nonrolling trim" is given approximately by the relation

$\frac{1}{2 \times \text{damping ratio}}$. This would give an amplification factor of 6.33 and 5.82 at resonance when $\delta_R = 1^\circ$ and 2°, respectively. These levels are indicated by the horizontal lines in the figure. However, it is obvious that transient effects are present in these examples, since the maxima lag the critical times somewhat and there are rapid oscillations after the maxima have been passed. These results are similar to those of Kanno, reference 9, for the spinning reentry body passing through resonance. In the present case the optimum time to traverse the resonance region is when the vehicle has the greatest restoring moment slope, so that the nonrolling trim is least, coupled with the greatest damping factor so that the amplification factor is smallest. The SHOT PUT was successfully flown with $\delta_R = 2^\circ$.

Wind Weighting

The necessity of a rigorous wind weighting analysis increases greatly with increasing launcher elevation angle and decreasing launcher length. The problem was investigated for the SHOT PUT vehicle on a zero length launcher by means of the six equations of motion with arbitrary wind. The goal was to obtain one simple chart which would give the elevation and azimuth corrections for the SHOT PUT vehicle for any wind condition. The details of the method, together with its assumptions are given fully by James, reference 10. Only the highlights of the method will be discussed here. It is believed that this method has fewer restrictions and greater ease of applicability in the field than any other method that has been reported in the literature.

In the analysis, it was assumed that the wind profile could be approximated by straight lines such as the curve labeled 40 ft/sec in figure 10. This profile has a 40 ft/sec surface velocity and a maximum value of 220 ft/sec at 42,000 feet. Other profiles were derived as simple linear submultiples of this one. The basic wind analysis was then performed in terms of these idealized profiles.

One result of the analysis was the usual vehicle sensitivity function. The vehicle is, of course, most sensitive to winds immediately after leaving the 2-inch launcher rail. The variation of sensitivity with altitude is indicated in the figure. At an altitude of 300 feet, the vehicle is only 1/3 as sensitive as it initially was. The sensitivity drops another third by 2,500 feet, but does not sensibly vanish until 42,000 feet, which corresponds to a time of 25 seconds. Thus, it was assumed that if, under the influence of any wind, the vehicle flight-path angles in pitch and yaw could be made the same as the no wind case at 25 seconds, the subsequent trajectories would differ only by the direct wind drift, which was negligible.

Shortly before the launch, the final launcher settings were determined by weighting the observed wind profile to determine its equivalent linear profile taking full account of the vehicle's varying sensitivity to disturbances up to 25 seconds. In the example in figure 10, the profiles shown as measured V_w and θ_w were determined to be equivalent to an idealized profile of 16.3 ft/sec and an azimuth of -145° relative to the down range axis. The correct launcher elevation and azimuth settings were then read immediately from a precomputed chart similar to figure 11. This figure shows the launcher elevation and azimuth correction angles for any weighted profile surface velocity and direction for the SHOT PUT vehicle, based on a no wind 78° elevation angle. The results of the previous figure are shown by the circular symbols. For a weighted profile surface velocity of 16.3 ft/sec and azimuth of -145°, the elevation correction is down 3.3° and the azimuth correction is right 9.0°. No time consuming iterations were involved during the countdown, since these were done when the chart was constructed several months before the launch. By keeping the time short between making the wind measurements and making the launcher adjustments, the chance of an appreciable change in the wind is lessened. For the SHOT PUT application this was an important advantage, since the vehicle had to be fired at a predetermined time with only a 5-minute tolerance.

This chart can also be used to test the validity of some important assumptions that are sometimes made in this problem. For example, some early analyses assumed that a direct sidewind has no effect on the flight-path angle in the pitch plane. The square symbols on the figure shows that a 40 ft/sec sidewind from the right requires a launcher elevation correction of 3.5° down. The reason for this result is of course the large azimuth change of 41° left required, bringing the wind around toward the tail. The resultant pitch up can only be eliminated by depressing the launcher. In this and subsequent examples, the example velocity of 40 ft/sec is used only for purposes of illustration. This does not mean that we regularly fired in such strong surface winds.

A second and related misconception is that the azimuth correction for a given wind can be computed for the nominal elevation angle and applied at all other elevation angles. Notice, however, from figure 11, that the azimuth correction is a strong function of elevation angle even though the sidewind component is the same. For a 40 ft/sec wind coming in at -45° from the nose (diamond symbol), the required elevation and azimuth corrections are 2.5° up and 52° right, respectively. Change the wind to 45° from the tail, or -135° (delta symbol), and the elevation correction is reduced to -8.0°, the azimuth correction is only 22° right. In both instances the sidewind component is the same, 28 ft/sec, but the 10.5° reduction in required launcher elevation causes a 30° decrease in azimuth correction. If the assumption being tested were correct, the lower part of the figure would be symmetrical about +90° and -90°, which it definitely is not.

A third limitation of some previous analyses is that the observed dispersion angle due to wind is applied directly to the launcher setting as the correction angle. This can lead to large errors as shown by the example in figure 12. For a tail wind of 40 ft/sec, the pitch dispersion angle is 18.5° up. The actual pitch correction angle from the previous figure is only 9.5°. For head and tail winds, the SHOT PUT correction angle is about 50 to 60 percent of the observed dispersion angle.

Lastly, many analyses assume a linear variation of the aerodynamic forces and moments with angle of attack. Consider a 40 ft/sec direct sidewind again. Obviously, at lift off, the angle of attack is 90°. The SHOT PUT vehicle would have to travel about 65 feet before the angle of attack decreased to 10°. In this distance, 20 percent of the total wind effect is experienced. Thus, high angle-of-attack aerodynamic data are needed for precise work.

The actual first-stage dispersions encountered in flying five of the SHOT PUT vehicles are summarized in figure 13. Here the data are in the form of angular dispersion in pitch and yaw at about 25 seconds. The results include dispersion due to all effects, including thrust misalignment. Four of the five points lie within the 1σ area; the point in the 2σ area was obtained from the first flight. In view of the sensitivity of the vehicle to the wind, these results indicate that the present system satisfactorily accounts for the important effects of wind on the trajectory, and that other disturbing effects were probably small.

In summary, the wind weighting and ascent dynamic stability problems of a sounding rocket have been satisfactorily solved by means of numerical solutions to the six equations of motion. The satisfactory determination of these numerical solutions required the use of modern high-speed computers, and accurate knowledge of the aerodynamic, inertia, and propulsion properties of the vehicle.

REFERENCES

1. Friedrich, Hans R., and Dore, Frank J.: The Dynamic Motion of a Missile Descending Through the Atmosphere. Jour. Aero. Sci., vol. 22, no. 9, Sept. 1955.

2. Zimmerman, C. H.: Theoretical Investigation of the Effect of Variations of Atmospheric Density With Time on the Stability of an Hypothetical Aircraft Having a Single Degree of Freedom. Thesis presented to Univ. of Virginia for Degree of Master of Aeronautical Engineering, June 1955.

3. Dornberger, Walter: V-2. Ballantine Books, 1954.

4. Phillips, William H.: Effect of Steady Rolling on Longitudinal and Directional Stability. NACA TN 1627, 1948.

5. Nicolaides, John D.: On the Free Flight Motion of Missiles Having Slight Configurational Asymmetries. Rep. No. 858, Ballistic Res. Labs., Aberdeen Proving Ground, June 1953.

6. Nelson, Robert L.: The Motions of Rolling Symmetrical Missiles Referred to a Body-Axis System. NACA TN 3737, 1956.

7. Enkenhus, K. R., and Bilodeau, P.: Tests on Resonating Models in the C.A.R.D.E. Aeroballistics Range. CARDE Technical Memorandum 158/58, 1958.

8. James, Robert L., Jr.: A Three-Dimensional Trajectory Simulation Using Six Degrees of Freedom With Arbitrary Wind. NASA TN D-641, 1961.

9. Kanno, D. S.: Spin-Induced Forced Resonant Behavior of a Ballistic Body Re-entering the Atmosphere. LMSD 288139, Jan. 1960.

10. James, Robert L., Jr., and Harris, Ronald J.: Calculation of Wind Compensation for Launching of Unguided Rockets. NASA TN D-645, 1961.

A. INERTIA TERMS — COMPLETE REPRESENTATION

B. FORCING FUNCTIONS

1. FORCES AND MOMENTS DUE TO ROCKET MOTOR THRUSTS

2. AERODYNAMIC FUNCTIONS

a. EQUAL STABILITY IN PITCH AND YAW

b. INVARIANT WITH AERODYNAMIC ROLL ANGLE

c. VARY WITH RESULTANT ANGLE OF ATTACK AND MACH NUMBER

d. ASYMMETRIES IN PITCH AND YAW AT α AND $\beta = 0$

NASA

Figure 1.- Important assumptions for equations of motion.

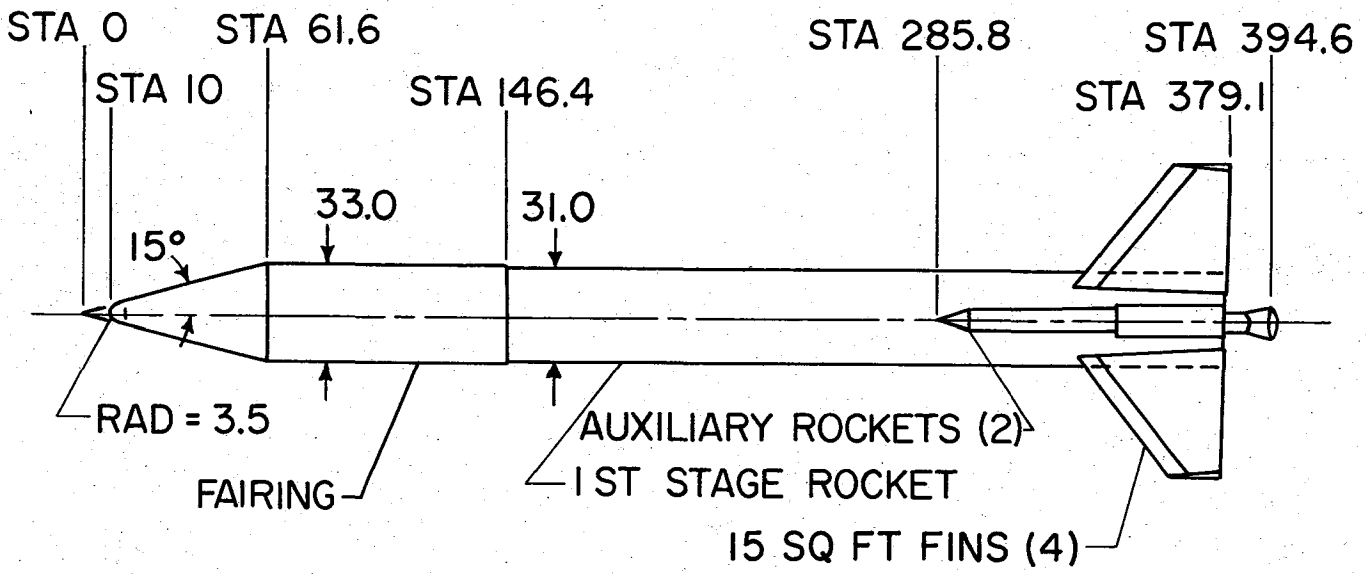

FIRST STAGE

ALL DIMENSIONS IN INCHES

WEIGHTS	IGNITION	BURNOUT
FIRST STAGE	11,200 LB	3,600 LB

NASA

Figure 2.- General configuration of the SHOT PUT vehicle.

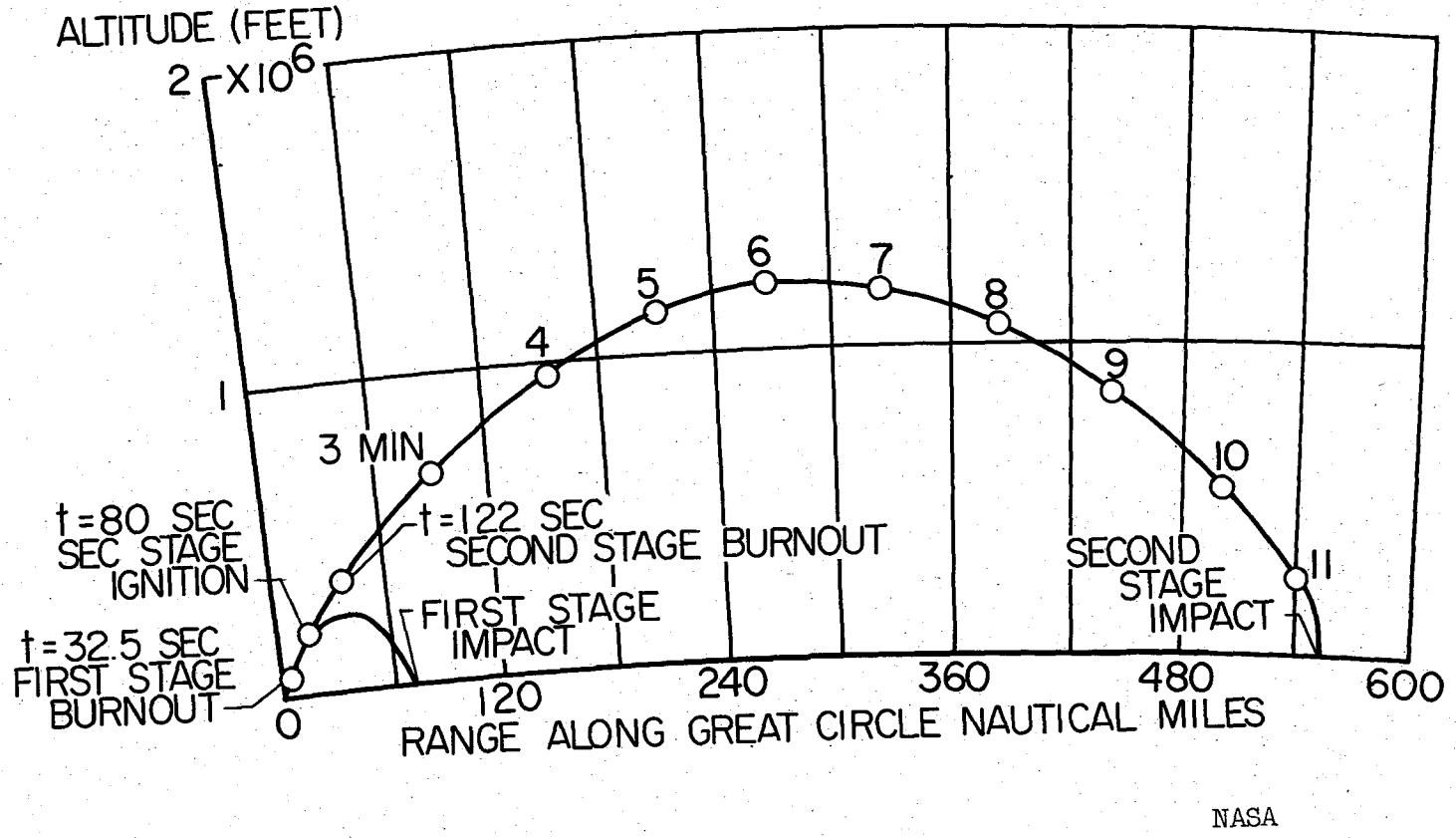

Figure 3.- SHOT PUT nominal trajectory in space.

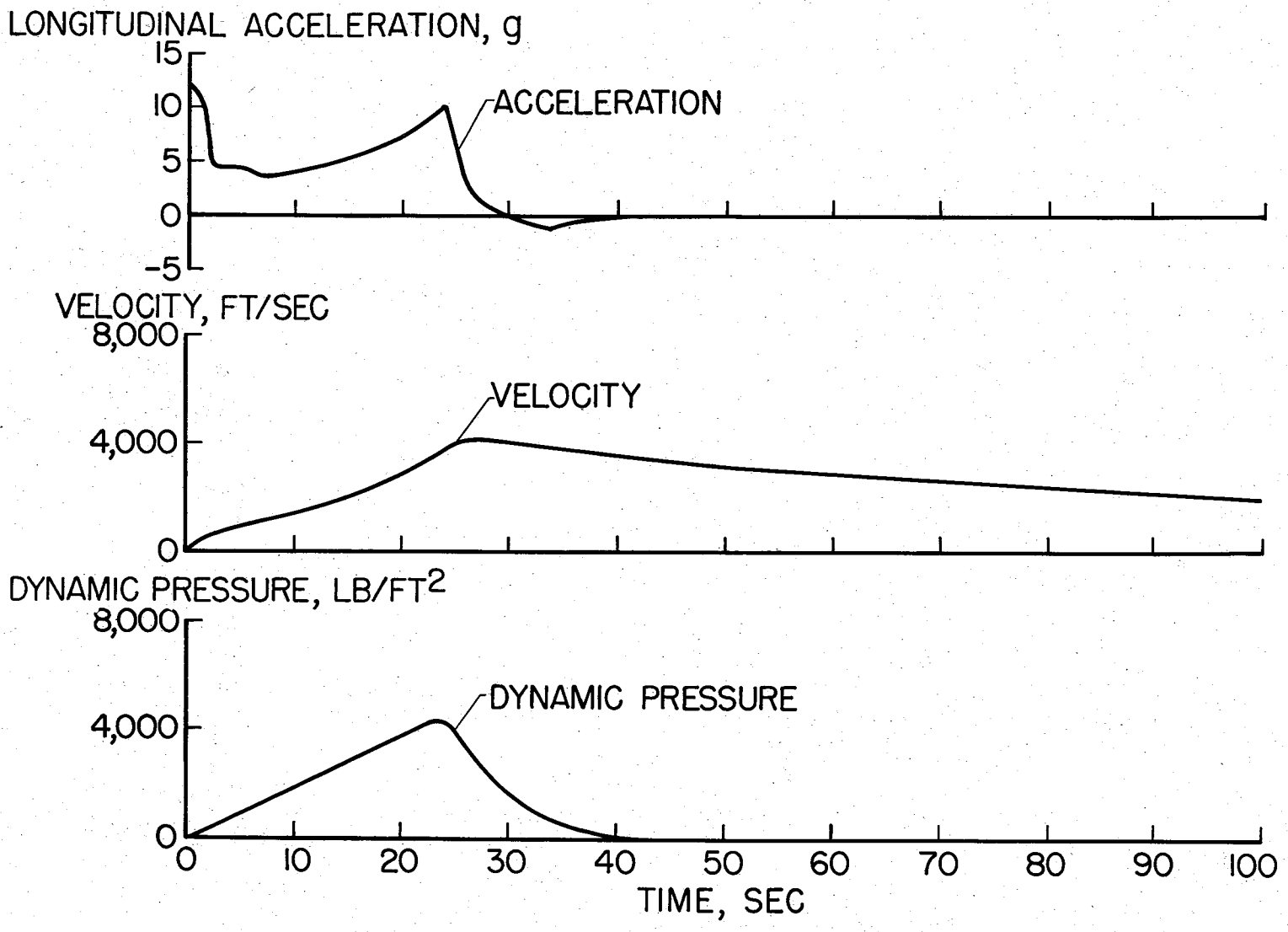

NASA

Figure 4.- SHOT PUT first-stage time histories.

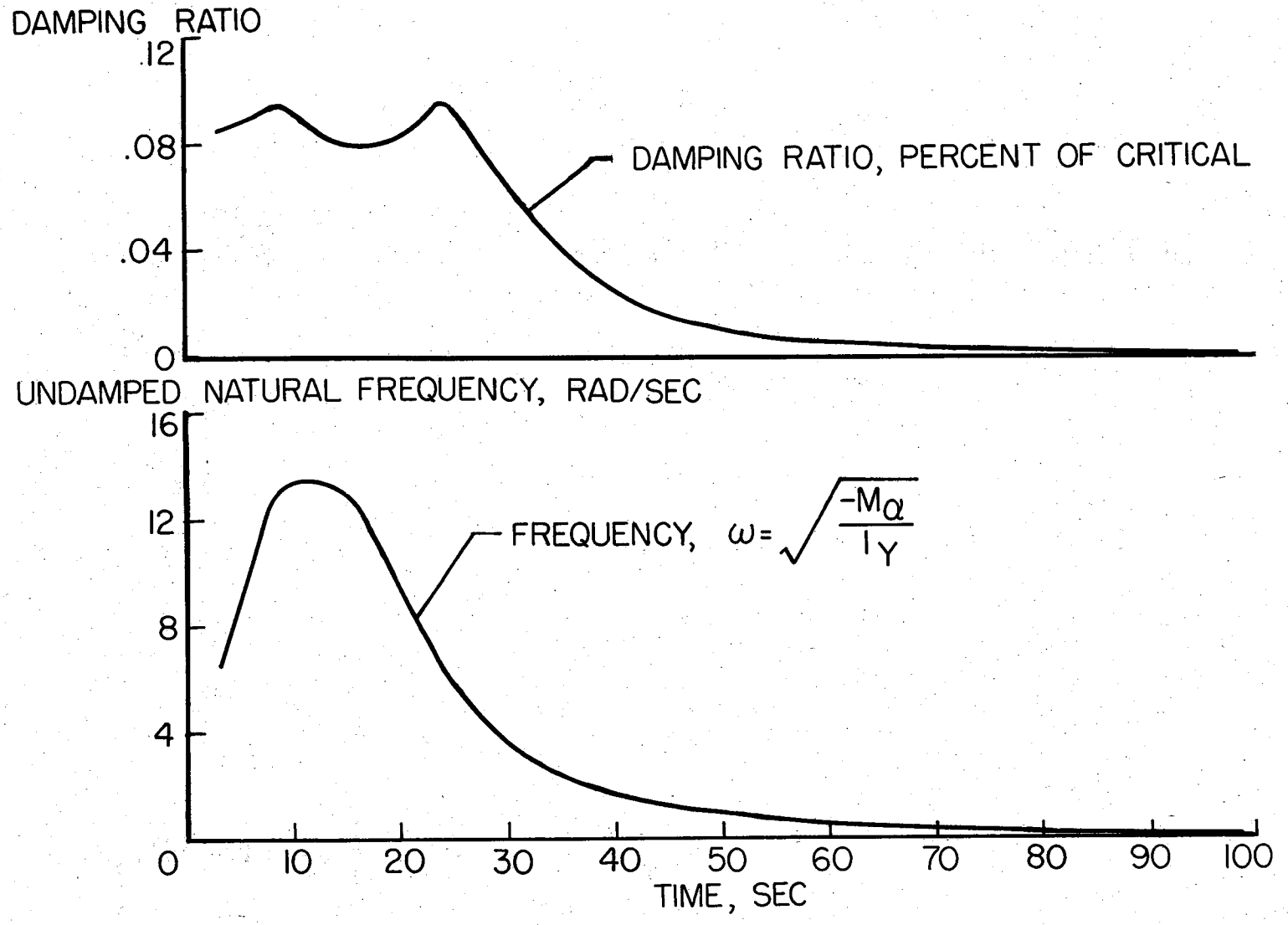

Figure 5.- SHOT PUT first-stage short-period characteristics.

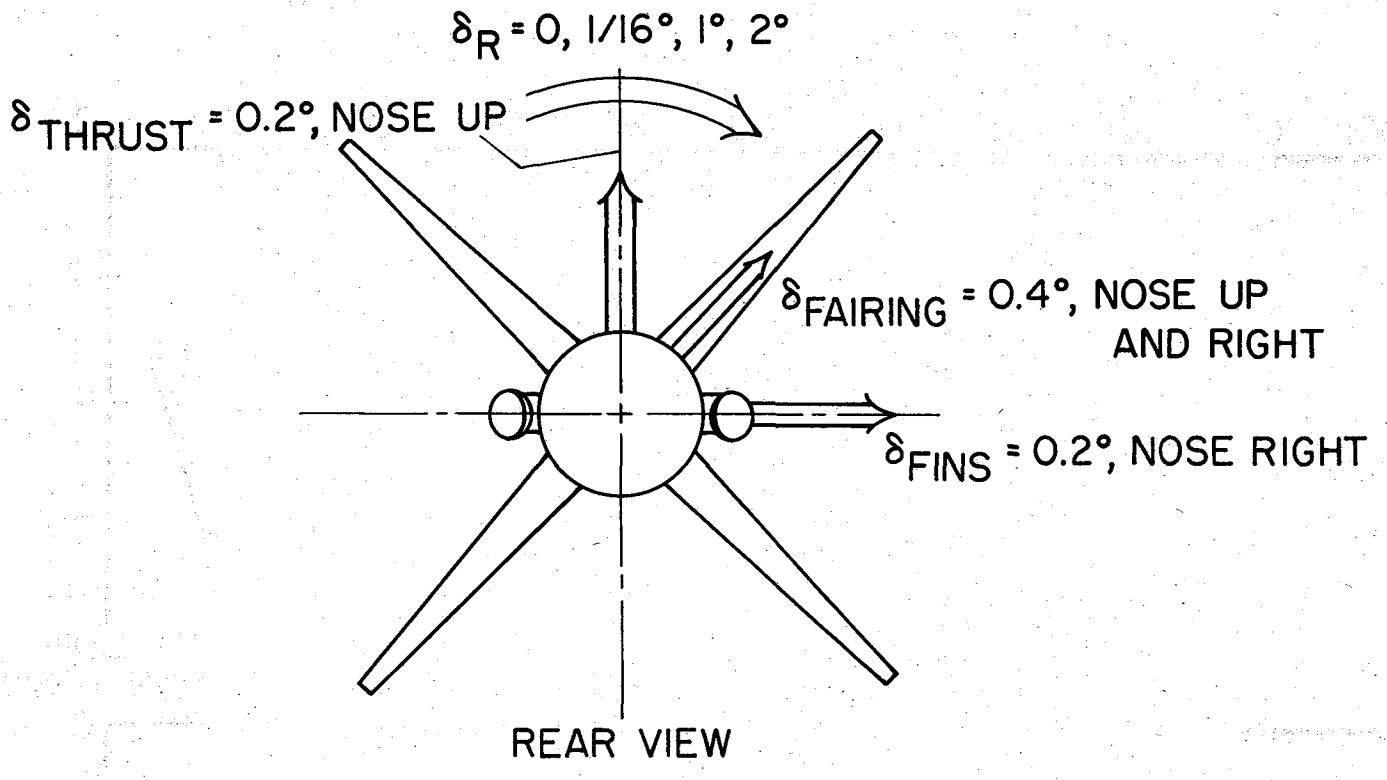

NOTE: ARROWS INDICATE DIRECTION OF ROTATION OF NOSE DUE TO ACTION OF INDICATED MISALIGNMENT

NASA

Figure 6.- Assumed asymmetries.

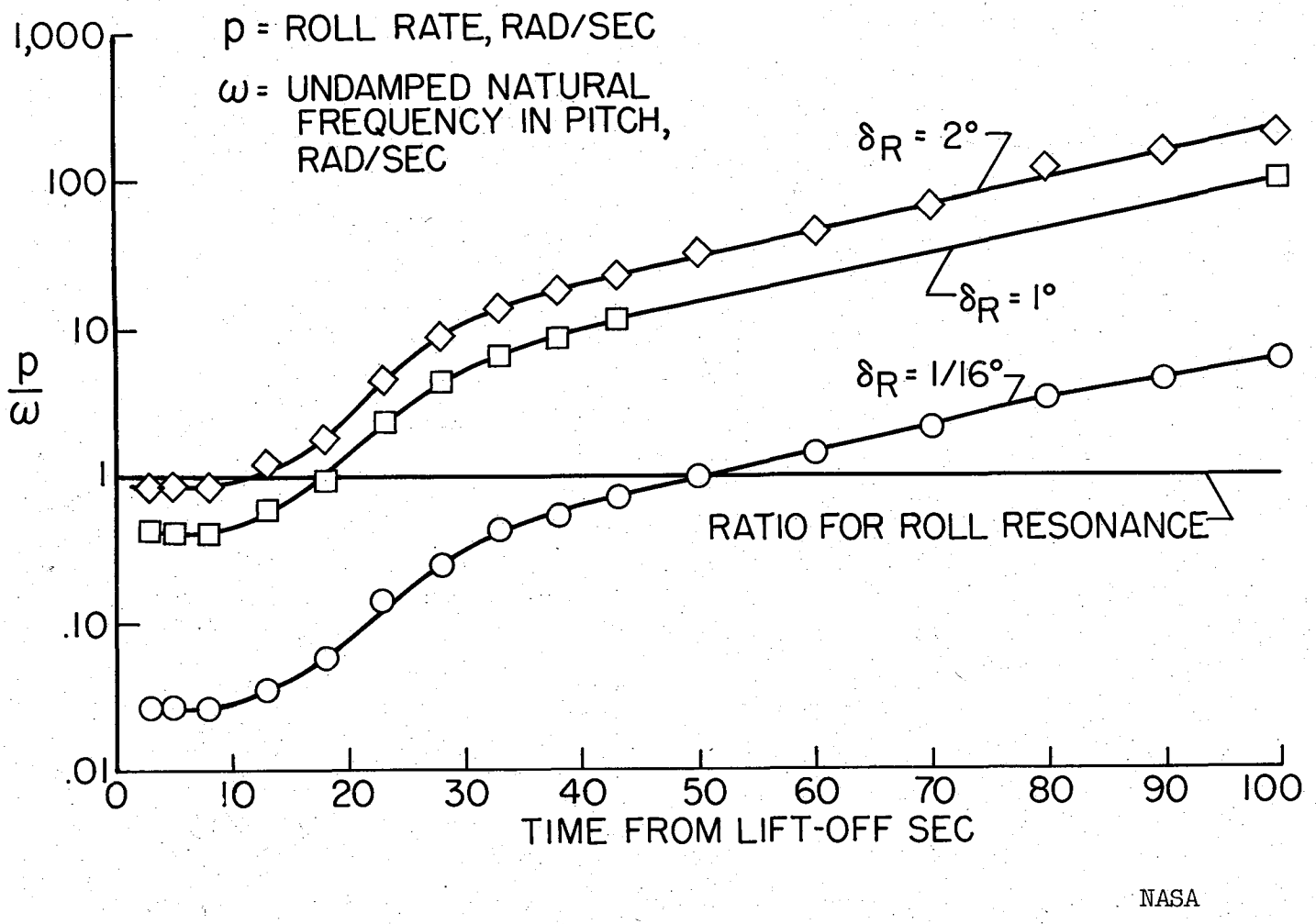

Figure 7.- Frequency ratios for SHOT PUT first stage.

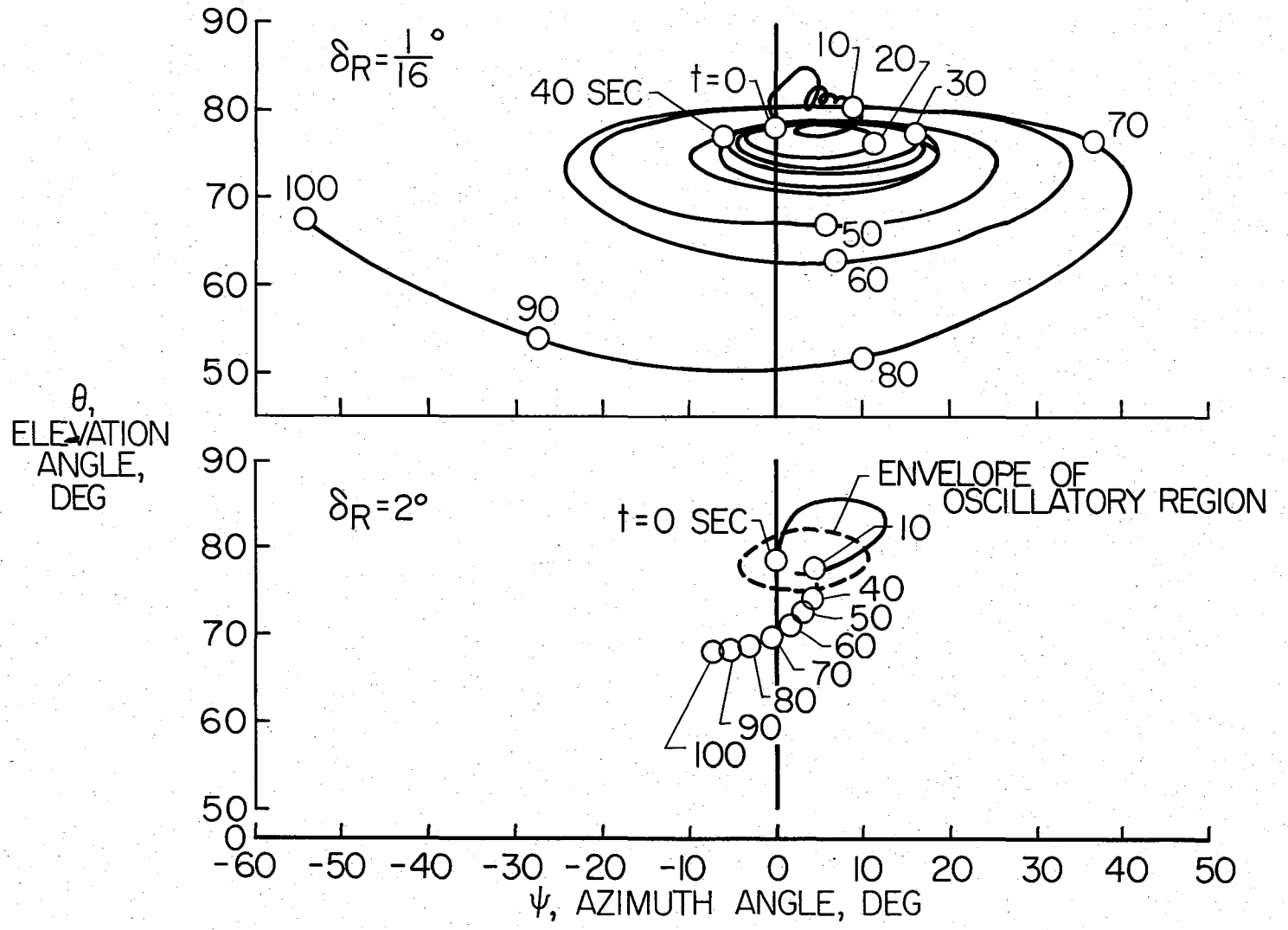

NASA

Figure 8.- First-stage space motions.

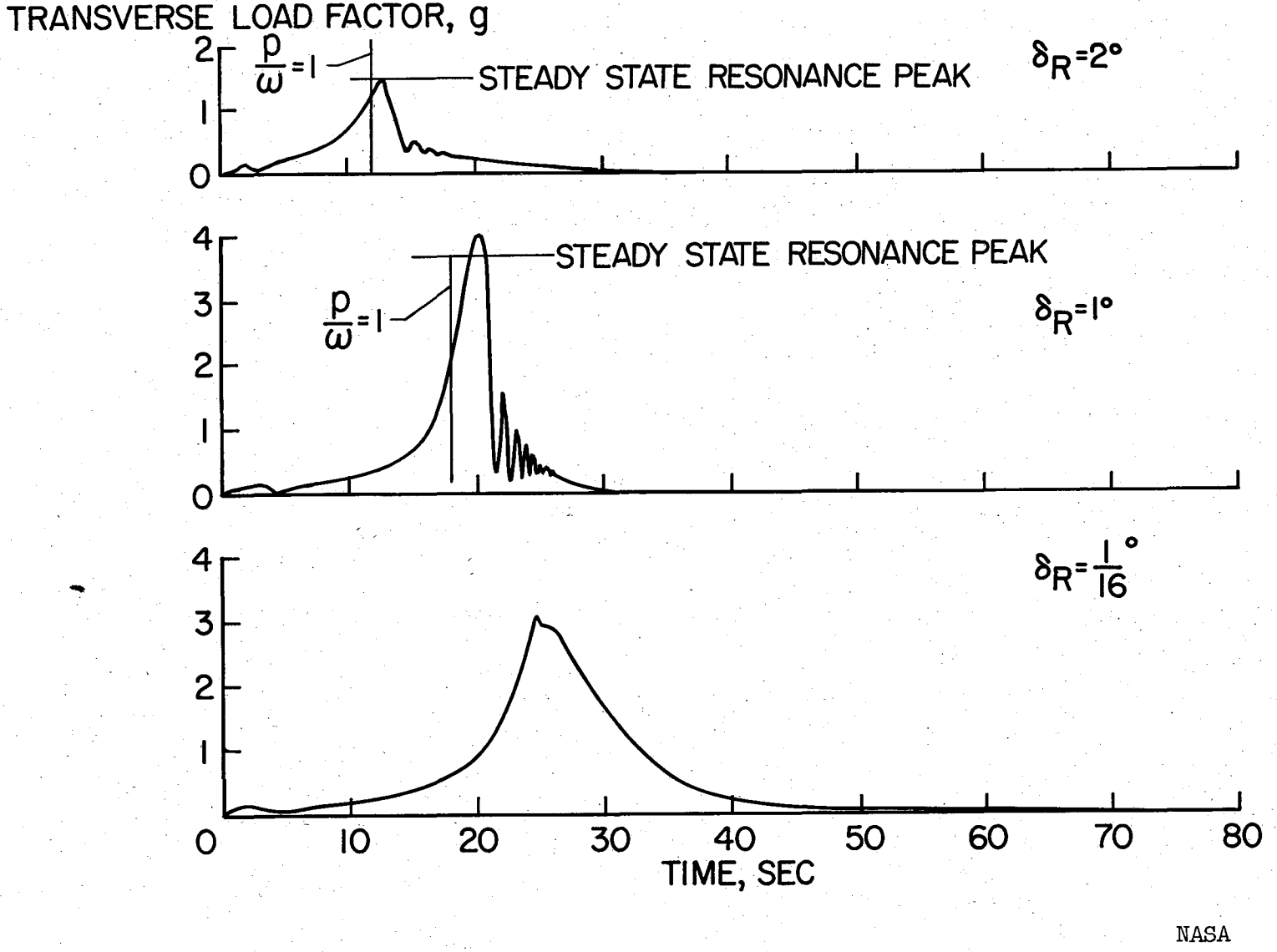

Figure 9.- Effect of roll deflections on first-stage loads.

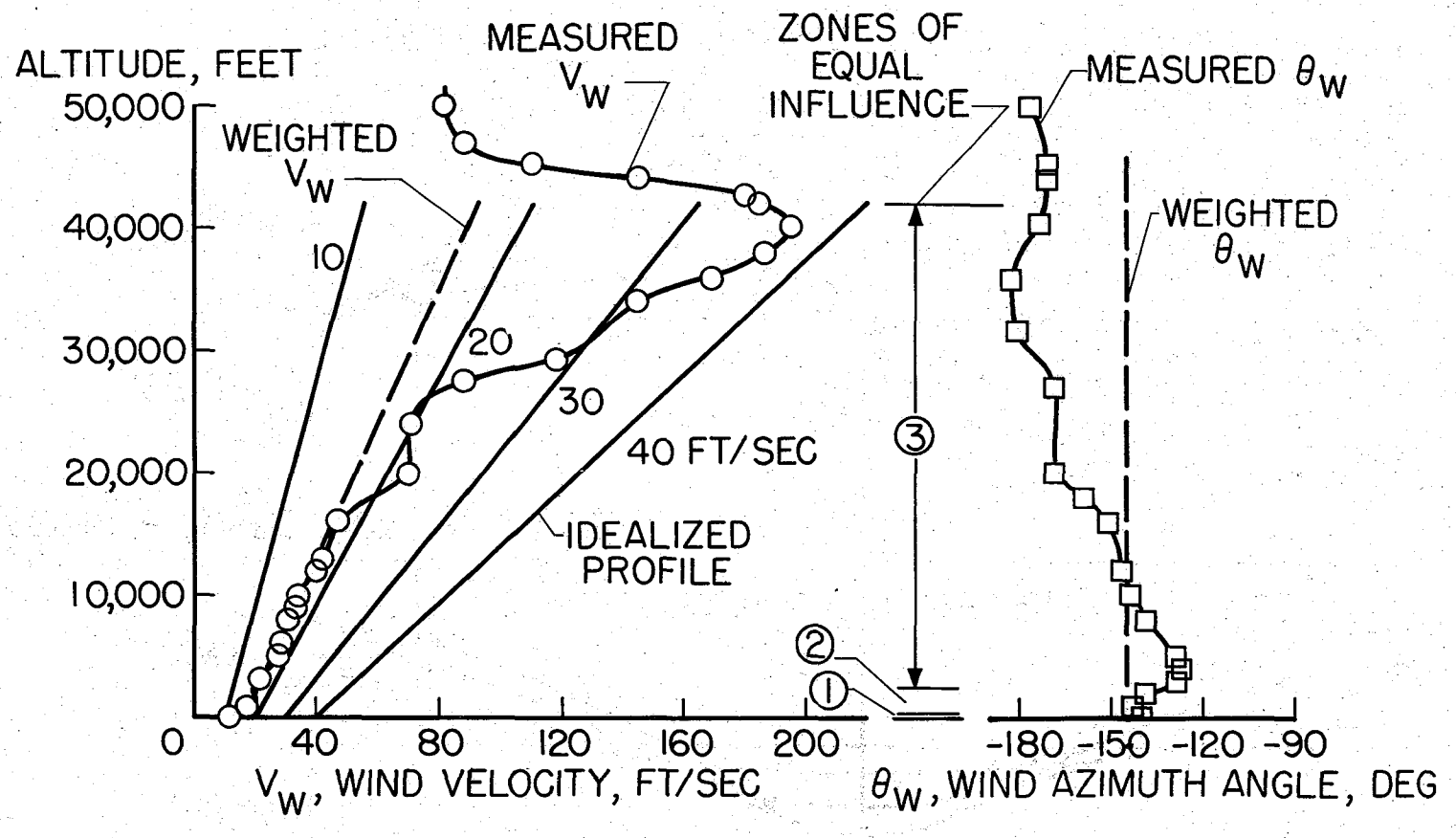

NASA

Figure 10.- Actual and idealized wind profiles.

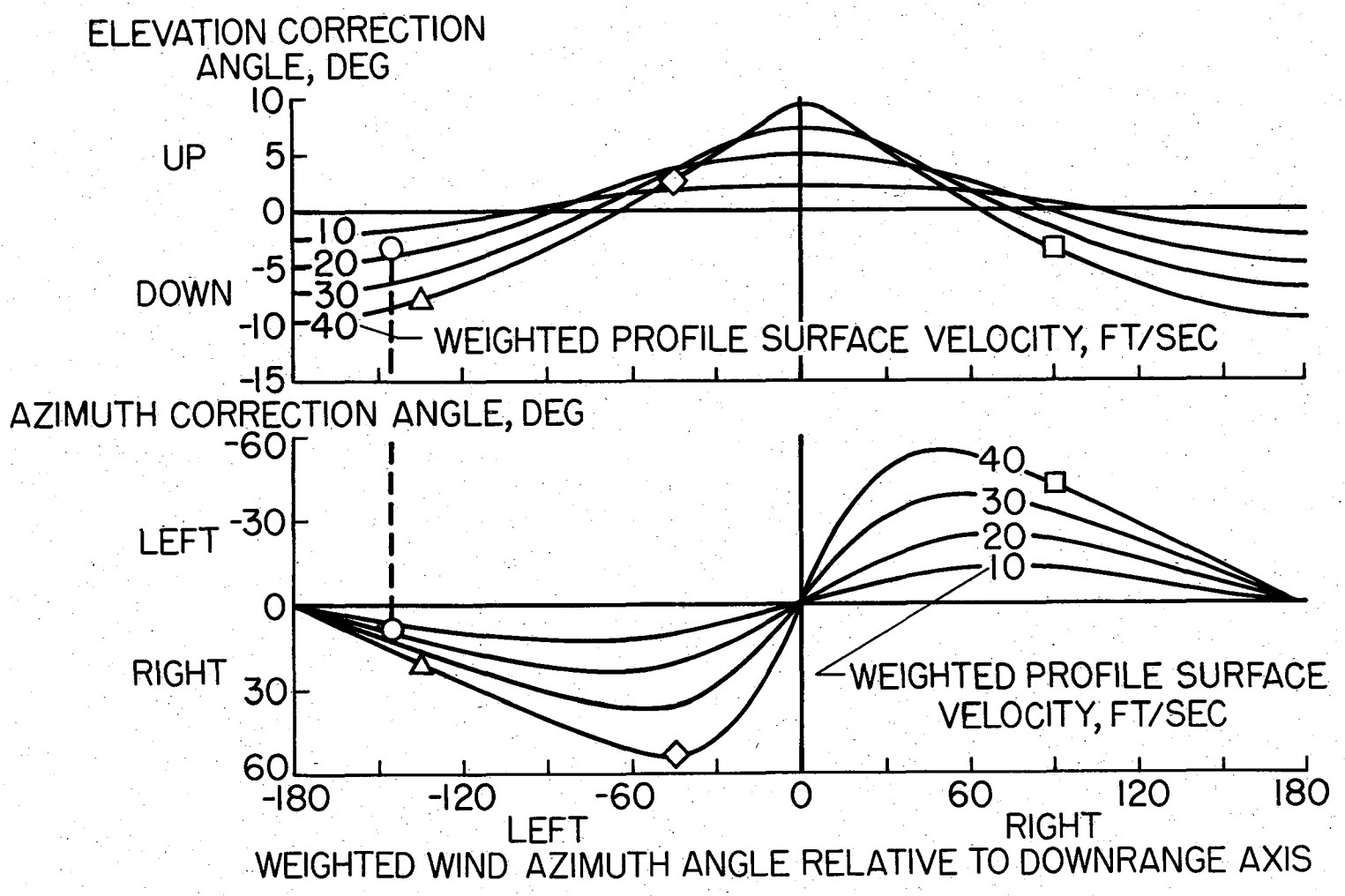

Figure 11.- Wind compensation for SHOT PUT.

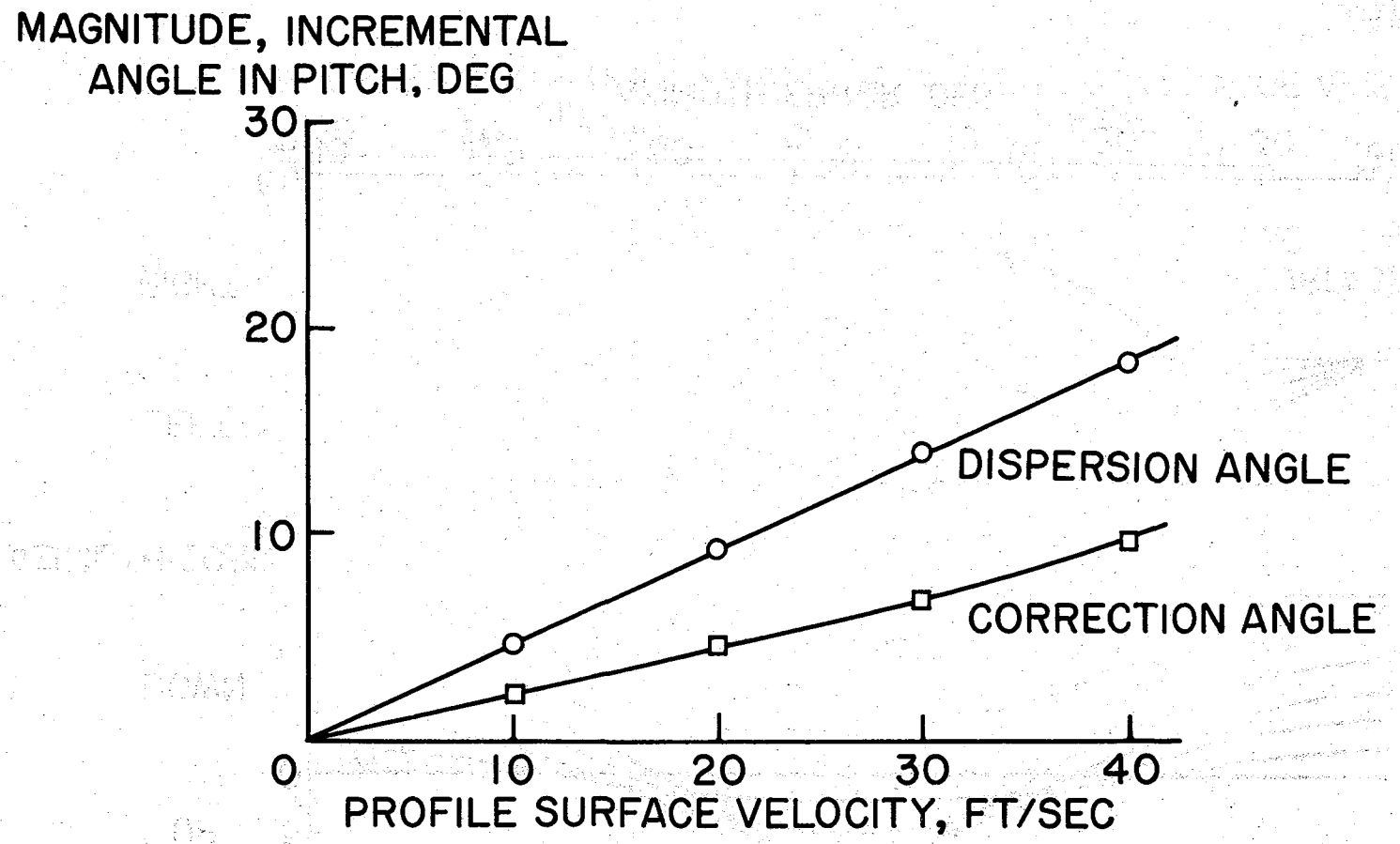

NASA

Figure 12.- SHOT PUT dispersion and correction angles.

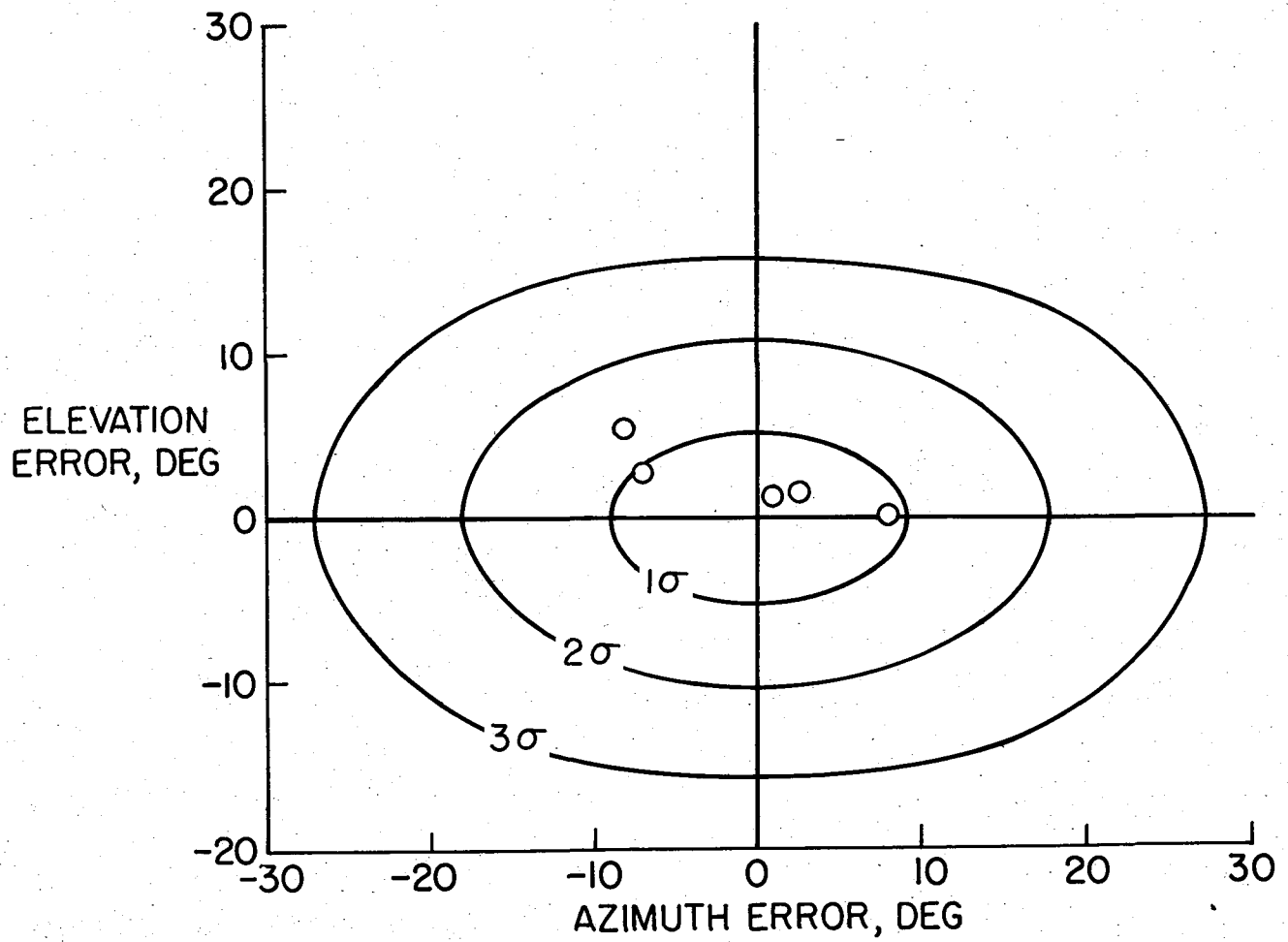

NASA

Figure 13.- Summary of SHOT PUT first-stage dispersion angles at t = 25 seconds.

NASA - Langley Field, Va. L-1749